

Interferometric Observation of the Highly Polarized SiO Maser Emission from the $v = 1, J = 5 - 4$ Transition Associated with VY Canis Majoris

Hiroko Shinnaga^{1,2}, James M. Moran³, Ken H. Young³, and Paul T.P. Ho³

hshinnaga@cfa.harvard.edu

ABSTRACT

We used the Submillimeter Array to image the SiO maser emission in the $v = 1, J = 5 - 4$ transition associated with the peculiar red supergiant VY Canis Majoris. We identified seven maser components and measured their relative positions and linear polarization properties. Five of the maser components are coincident to within about 150 mas (~ 200 AU at the distance of 1.5 kpc); most of them may originate in the circumstellar envelope at a radius of about 50 mas from the star along with the SiO masers in the lowest rotational transitions. Our measurements show that two of the maser components may be offset from the inner stellar envelope (at the 3σ level of significance) and may be part of a larger bipolar outflow associated with VY CMa identified by Shinnaga et al. The strongest maser feature at a velocity of 35.9 kms^{-1} has a 60 percent linear polarization, and its polarization direction is aligned with the bipolar axis. Such a high degree of polarization suggests that maser inversion is due to radiative pumping. Five of the other maser features have significant linear polarization.

Subject headings: masers — polarization — techniques: interferometric — stars: late-type — stars: individual (VY Canis Majoris) — radio lines: general

1. INTRODUCTION

The unusual star VY Canis Majoris (VY CMa), is located at the edge of the very large ($\sim 5^\circ$ in diameter) Sharpless 310 HII region at a distance of 1.5 kpc (e.g. Herbig (1970);

¹Harvard-Smithsonian Center for Astrophysics, Submillimeter Array, 645 North A'ohoku Place, Hilo, HI 96720 USA

²Present address: California Institute of Technology Submillimeter Observatory, 111 Nowelo Street, Hilo, HI 96720 USA

³Harvard-Smithsonian Center for Astrophysics, 60 Garden Street, Cambridge, MA 02138, USA

Lada & Reid (1978)), and is one of the most intrinsically luminous stars known in the Galaxy with $L_* \sim (2 - 5) \times 10^5 L_\odot$ (e.g. Le Sidaner & Le Bertre (1996)). Despite its high luminosity, it has a low effective temperature of $T_* \sim 2800$ K, making it a red supergiant of spectral class M5Ib with a mass of $\sim 25 M_\odot$. Its unusually high mass loss rate for a red supergiant, $\dot{M}_* \sim (1 - 3) \times 10^{-4} M_\odot \text{ yr}^{-1}$ (Jura & Kleinmann 1990), is consistent with its thick circumstellar envelope and suggests that VY CMa may be close to the end of its life cycle. High resolution images taken at optical and infrared wavelengths reveal complicated circumstellar dust structures (Monnier et al. 1999; Smith et al. 2001). However, it is difficult to investigate the innermost circumstellar structures via the continuum emission because of the high opacity.

VY CMa’s extended outflowing envelope is traced by various species of molecular masers that conform to the standard paradigm for late type and supergiant stars whereby various species trace specific layers of the envelope for reasons involving density and excitation process (e.g., Moran et al. (1977); Reid & Muhleman (1978); Marvel, Diamond, & Kemball (1998); Shinnaga et al. (2003); Miyoshi (2003)). One of the unusual characteristics of the emission from the circumstellar envelope is the high degree of linear polarization in the SiO $v = 0$ lines. The only other stars that are known to show polarization in the SiO ground state are R Cas (Shinnaga, Tsuboi, & Kasuga 2002) and Orion KL/IRC2 source I (Tsuboi et al. 1996).

We report the first imaging for the $v = 1$, $J = 5 - 4$ transition with high angular resolution and also describe the spectral characteristics of the strong linear polarization detected in this line.

2. OBSERVATIONS AND DATA REDUCTION

Observations of the SiO emissions in the $v = 1$, $J = 5 - 4$ transition (215.595950 GHz) towards VY CMa were made with the partially completed *Submillimeter Array*¹ (SMA; Ho, Moran, & Lo (2004)), located on Mauna Kea, on 7 December 2002 under fair weather conditions (the zenith opacity $\tau_{225\text{GHz}} \sim 0.15 - 0.2$). The phase tracking center was set at RA = $07^h 22^m 58.^s27$, Decl. = $-25^\circ 46' 03.''4$ (J2000) and the field of view (FOV) was $57''$. A compact configuration (baselines ranging from 6.3 to 18.1 k λ) with three antennas was employed for imaging the maser line. The beam size was $13.9'' \times 5.6''$. The spectral

¹The Submillimeter Array is a joint project between the Smithsonian Astrophysical Observatory and the Academia Sinica Institute of Astronomy and Astrophysics, and is funded by the Smithsonian Institution and the Academia Sinica.

window was centered at 10.0 km s^{-1} in V_{LSR} . The frequency resolution was $\sim 400 \text{ kHz}$. The typical double sideband system temperature was 500 K. We observed VY CMa along with a relatively bright nearby quasar, 0727–115 ($\sim 14^\circ$ away), for the relative amplitude and astrometric phase calibration, and Callisto for the absolute flux calibration. Precise phase calibration was achieved through the use of the maser component at 35.9 km s^{-1} as a phase reference. The passband calibration was done on Jupiter. Visibility data were calculated with the MIR IDL package (Scoville et al. 1993). The quasar amplitude showed no systematic variation with random fluctuation less than $\sim 10\%$ of the mean value, which reflects the accuracy of the amplitude calibration.

Linear polarization measurements were accomplished by taking advantage of the diurnal rotation of the sky with respect to the axis of polarization sensitivity of the Array. The SMA antennas have alt-azimuth mounts, and the receivers, mounted at the Nasmyth focus following reflections from five intermediate mirrors, have fixed linearly polarized feeds. The final reflection before the receiver is achieved with a wire grid, which ensures that the overall polarization purity is better than 20 db. Because of the Nasmyth optics, the plane of the receiver polarization outside the antenna with respect to the local vertical is $45 - EL$, where EL is the elevation angle of the source. The feed position angle on the celestial frame is (e.g., Smart (1962))

$$PA(\text{deg}) = 45 - EL + \sin \frac{\cos(\phi_{\text{LAT}}) \cdot \sin(HA)}{\cos(EL)} \quad (1)$$

where ϕ is the latitude of the Array ($\sim 19^\circ 49' 27''$) and HA is the source hour angle. In our experiment, HA ranged from -3 hours to 2.5 hours and PA ranged from -25 to 60° , which was sufficient to determine the linear polarization characteristics of the maser emission.

3. ANALYSIS, RESULTS, AND DISCUSSION

3.1. Line profile and linear polarization of the maser

Figure 1 shows an integrated spectrum (vector average of all spectra) of the SiO high J maser ($v = 1$, $J = 5 - 4$). The noise level in the spectrum was 1.1 Jy. Seven major velocity components have been identified by the number in the figure. In addition to these, we also detected two weak high velocity components at the red shifted edge, at $V_{\text{LSR}} \sim 48$ and $\sim 56 \text{ km s}^{-1}$. The brightest maser, component 2, has a very narrow line width ($< 0.5 \text{ km s}^{-1}$ at full width at half maximum) corresponding to a thermal Doppler width of about 600K if the maser is saturated. The line profile of the high J transition is quite different from those of the lower J transitions (e.g., Shinnaga, Tsuboi, & Kasuga (1999)), indicating different

regions for their origins.

Figure 2 the flux densities of the seven major components at each PA . To determine the polarization of the masers, we fit the flux density of each maser component, S_k , as a function of PA to the equation

$$S_k = S_{0_k} + S_{p_k} \cos[2(PA - \psi_k)] \quad (2)$$

where S_{0_k} is the average flux density of maser component k , S_{p_k} is the polarized flux density, and ψ_k is the position angle of the linear polarization. Table 1 shows the results of this analysis. The fractional linear polarization, listed in the rightmost column of Table 1, is given by S_{p_k}/S_{0_k} . The fractional polarization percentages ranged from less than 10 percent (component 5) to about 60 percent (components 1 and 2). These values of fractional polarization are lower limits to the total polarization, since our measurement technique was not sensitive to circular polarization.

Since component 5 showed no measurable change in flux density over the 5.5 hour duration of the observations, we are confident that the gain of the SMA was correctly calibrated throughout the experiment by the normal calibration on the nearby quasar, and that this component has no measurable linear polarization. To check this conclusion, and possibly improve the gain calibration, we performed the following analysis. After the linear analysis (based on Eq. (2)) to determine the three polarization parameters for each maser component, we examined the residuals at each time (PA). We estimated a gain factor correction for each time (six parameters) to minimize the overall deviations. We then solved again for the polarization parameters, and iterated the process several times. The solution converged quickly and stably, yielding the six gain factors: 1.00, 1.00, 1.04, 0.94, 0.99, and 1.03. The final polarization parameters were not significantly different from those obtained in the first iteration (i.e., gain factors set to unity). The iterative solution reduced the overall rms noise level by about 20 percent and reduced the χ^2 to essentially unity. This demonstrates that the measurement of the polarization parameters are accurate to within the quoted errors and are not subject to systematic errors due to calibration errors in the gain of the Array. It also shows that the *a priori* gain calibration based on the interleaved quasar observations was quite good, and validates the implicit assumption that the maser components did not vary intrinsically by more than a few percent over the period of observations.

We tested the hypothesis that the polarization angles of the maser spots are the same. Under this assumption, the weighted mean polarization angle is $72 \pm 4^\circ$. The reduced χ^2 is 1.13, which strongly suggests that the polarization angles are the same and that the deviations from the mean of the position angles are not significant, except possibly for components 3 and 6, which each deviate by about 1.5σ .

3.2. Angular distribution of the maser spots

We assume that the individual masers components are unresolved by the SMA because their intrinsic sizes are less than ten milliarcsecond (e.g., see Reid & Moran (1986) for discussion of maser angular sizes). We tried to measure the angular distribution of maser spots with respect to the strongest maser component 2. To estimate the positions, we made an image for each spectral channel and fit it with a two dimensional Gaussian function, using AIPS tasks IMFIT and JMFIT. To improve the component position error estimates, we averaged the results over several channels that contributed to the maser emission of each spot. Note that, for a point source, the determination of the peak of the image is statistically equivalent to a χ^2 fitting of the phases (e.g. Thompson, Moran, & Swenson (2001)). In particular, since the analysis is based on the assumption that the individual maser components are point sources, the fact that the synthesized beam had high sidelobes was not important. Note that the visibility amplitude variations due to polarization do not bias the position estimate.

Since we referenced the phase of each maser to the phase of the reference feature, the effects of any systematic errors were eliminated to first order. Any random phase errors between channels were reflected in the formal position errors. However, any systematic phase drifts between channels, caused by delay changes or electronic changes in the filter responses could have affected the measured positions. We have analyzed the phase versus time data for the reference quasar, spectrally resolved into four channels, and we found no evidence for any relative phase changes at the limit of about two degrees, which was limited by the measurement noise. The electronic stability and delay calibration of the system suggest that the relative phase changes are much smaller than this amount. A two degree systematic error would produce an error of less than $0.02''$ in relative position.

Table 1 lists the positions of the masers, the relevant velocity ranges, and the measurement errors. The errors are close to the expected levels predicted by the formula $\delta\theta = 0.5BW/\text{snr}$ (e.g. Kogan (1996)), where BW is the beamwidth in direction of RA or Decl., and snr is the signal-to-noise ratio. The snr of each component is its flux density divided by the measured noise of 1.10 Jy obtained from the integrated spectrum.

Masers 3, 4, 5, and 7 are coincident with maser 2 within the $1-\sigma$ error bars (150 mas in each coordinate or 200 AU). These masers are most likely associated with the SiO masers in the circumstellar shell at radius of 50 AU. Higher resolution measurements are needed to determine their exact positions in the shell. Masers 1 and 6 are offset in declination by 1300 mas (2.5σ) and 500 mas (4σ), respectively. These offsets might be real, but clearly have only marginal significance. Although there appear to be no $J = 1 - 0$ transition masers beyond the 50 mas shell (Miyoshi 2003), it is conceivable that masers could exist in the

high J transitions in the bipolar outflow due to shock excitation. Masers 1 and 6 could be manifestations of such shocks.

The positions of the maser spots are plotted in Figure 3, with the polarization indicated on each spot. We have placed component 2 between the two outflow lobes at the position set by the central star. If the assumption is correct, the uncertainty of the relative alignment of the two images is $\lesssim 0.1''$. The relative alignment of the $v = 0$ image and our maser image is uncertain to $\lesssim 0.5''$, based on the positions of the reference quasars observed in these two measurements. Note that the position angle of the polarization of maser component 2 ($71 \pm 5^\circ$) and that of the mean of all the components ($72 \pm 4^\circ$) are nearly aligned with the outflow. This correlation suggests a relationship between the circumstellar envelope and the more extended bipolar outflow. Note that since the components are on both sides of the systemic velocity, they arise in both the approaching and receding sides of the envelopes.

3.3. Continuum measurement

We imaged the continuum emission in the line free channels. Because of the poor beamshape of the Array, we could not determine the spatial structure of the continuum. However, we measured the total flux density to be 270 ± 40 mJy. The flux at 301 GHz and 658 GHz measured with the SMA recently were 340 ± 10 mJy and 7.8 ± 2.6 Jy, respectively. The SED obtained by combining our results with other measurements in the submillimeter band (Marshall, Leahy, & Kwok 1992; Sopka et al. 1985) give a spectral index for flux density of about -3.0 for the frequency range 200 – 750 GHz. The emission is clearly almost entirely due to dust, with a small contribution from the star. The spectral index is slightly less (-2.5) over the range 1,000 – 15,000 GHz (300 – 20 microns) (Le Sidaner & Le Bertre 1996).

4. Pumping Mechanism of the SiO High J Maser

Two theories have been proposed to explain the SiO maser pumping mechanism, especially for the low J transitions: radiative pumping (Kwan & Scoville 1974; Deguchi & Iguchi 1976; Bujarrabal 1994a) and collisional pumping (Elitzur 1980; Doel et al. 1995). The positional coincidence of emission among different $v \geq 1$ vibrational states as observed with KNIFE (Miyoshi et al. 1994) seems to support the collisional pumping theory.

On the other hand, the 60% linear polarization that we observe suggests radiative pumping (Nedoluha & Watson 1990). A fractional polarization this high for the $J = 5-4$ transition apparently requires anisotropy in the angular distribution of the IR radiation involved in de-

termining the populations of the masing states (Western & Watson 1984). This anisotropy could occur, in principle, for either collisional (through the escaping IR radiation) or radiative pumping. However, it occurs more naturally for radiative pumping since the incident IR radiation comes from the direction of the star, and is a larger effect in this case (Western & Watson 1983). Note that most theoretical analyses predict lower polarization in the higher J transitions, contrary to observations.

The polarization direction of the radiation would be parallel or perpendicular to the magnetic field if $g\Omega > R, \Gamma$, where $g\Omega$ is the Zeeman rate, $1.5 \text{ rad s}^{-1} \text{ mG}^{-1}$, Γ is the maser level decay rate, about 5 s^{-1} , and R is stimulated emission rate, $4 \times 10^{-6} T_b \Omega_m$, where T_b is the brightness temperature and Ω_m is the maser beam angle (Goldreich, Keeley, & Kwan 1973). Otherwise, the polarization would be aligned with the direction of the pump anisotropy. The VLBA image of the SiO masers in the $v = 1, J = 1 - 0$ transition suggest that the spot sizes are about 2 mas (about 2 AU) (Miyoshi 2003), so the maximum brightness temperature is about $4 \times 10^8 \text{ K}$. Taking $\Omega_m = 10^{-2}$ (e.g., Reid & Moran (1986)), the masers satisfy the $g\Omega > R$ criterion if $B > 10 \text{ mG}$. Since the magnetic field in the water masers in VY CMa has been estimated to be about 150 mG, based on a Zeeman interpretation of the observed circular polarization (Vlemmings, Diamond, & van Langevelde 2002), polarization would be expected to trace the magnetic field. Note that well ordered magnetic fields have been seen in other SiO masers (e.g. VY CMa: Shinnaga et al. (2003), TX Cam: Kemball & Diamond (1997)).

We thank all SMA team members for their enthusiastic work and the Hawaiian people for allowing us to use their sacred mountain, Mauna Kea. We are grateful to Raymond Blundell, Shuji Deguchi, Ray Furuya, Liz Humphreys, Makoto Miyoshi, Scott Paine, and William Watson for helpful discussions.

REFERENCES

- Bujarrabal, V. 1994, A&A, 285, 971
- Deguchi, S. & Iguchi, T. 1976, PASJ, 28, 307
- Doel, R. C., Gray, M. D., Humphreys, E. M. L., Braithwaite, M. F., & Field, D. 1995, A&A, 302, 797
- Elitzur, M. 1980, ApJ, 240, 553
- Goldreich, P., Keeley, D. A., & Kwan, J. Y. 1973, ApJ, 179, 111

- Herbig, G. H. 1970, ApJ, 162, 557
- Ho, P. T. P., Moran, J. M. & Lo, K. Y. 2003, ApJ, in press (this issue)
- Jura, M. & Kleinmann, S. G. 1990, ApJS, 73, 769
- Kemball, A. J. & Diamond, P. J. 1997, ApJ, 481, L111
- Kogan, L. 1996, NRAO AIPS Memo. Ser. 92
- Kwan, J. & Scoville, N. 1974, ApJ, 194, L97
- Lada, C. J. & Reid, M. J. 1978, ApJ, 219, 95
- Le Sidaner, P. & Le Bertre, T. 1996, A&A, 314, 896
- Marshall, C. R., Leahy, D. A., & Kwok, S. 1992, PASP, 104, 397
- Marvel, K. B., Diamond, P. J., & Kemball, A. J. 1998, ASP Conf. Ser. 154: Cool Stars, Stellar Systems, and the Sun, 10, 1621
- Miyoshi, M., Matsumoto, K., Kamenno, S. et al. 1994, Nature, 371, 29
- Miyoshi, M. 2003, ASSL Vol. 283: Mass-Losing Pulsating Stars and their Circumstellar Matter, 303
- Monnier, J. D., Tuthill, P. G., Lopez, B., Cruzalebes, P., Danchi, W. C., & Haniff, C. A. 1999, ApJ, 512, 351
- Moran, J. M., Ball, J. A., Yen, J. L., Schwartz, P. R., Johnston, K. J., & Knowles, S. H. 1977, ApJ, 211, 160
- Nedoluha, G. E. & Watson, W. D. 1990, ApJ, 361, L53
- Reid, M. J. & Muhleman, D. O. 1978, ApJ, 220, 229
- Reid, M., & Moran, J. 1986, in Galactic and Extragalactic Radio Astronomy, eds. G. L. Verschuur & K. I. Kellermann (Springer-Verlag), 255
- Scoville, N. Z., Carlstrom, J. E., Chandler, C. J., Phillips, J. A., Scott, S. L., Tilanus, R. P. J., & Wang, Z. 1993, PASP, 105, 1482
- Shinnaga, H., Tsuboi, M., & Kasuga, T. 1999, PASJ, 51, 175
- Shinnaga, H., Tsuboi, M., & Kasuga, T. 2002, IAU Symposium, 206, 278

- Shinnaga, H., Claussen, M. J., Lim, J., Dinh-van-Trung, & Tsuboi, M. 2003, ASSL Vol. 283: Mass-Losing Pulsating Stars and their Circumstellar Matter, 393
- Smart, W. M., Spherical Astronomy, Cambridge U. Press (Cambridge)
- Smith, N., Humphreys, R. M., Davidson, K., Gehrz, R. D., Schuster, M. T., & Krautter, J. 2001, AJ, 121, 1111
- Sopka, R. J., Hildebrand, R., Jaffe, D. T., Gatley, I., Roellig, T., Werner, M., Jura, M., & Zuckerman, B. 1985, ApJ, 294, 242
- Thompson, A., Moran, J., & Swenson, G. Interferometry and Synthesis in Radio Astronomy, 2001 (Wiley, Second ed.)
- Tsuboi, M., Ohta, E., Kasuga, T., Murata, Y., & Handa, T. 1996, ApJ, 461, L107
- Western, L. R. & Watson, W. D. 1983, ApJ, 275, 195
- Western, L. R. & Watson, W. D. 1984, ApJ, 285, 158
- Vlemmings, W. H. T., Diamond, P. J., & van Langevelde, H. J.(2002) 2002, A&A, 394, 589

Table 1. Parameters of Seven Maser Components

Number	Velocity ^a (kms ⁻¹)	Velocity ^b Range	Peak Intensity (Jy)	X Offset ^c (arcsec)	Y Offset ^c (arcsec)	PA (degrees)	Degree of Linear Polarization (%)
1	42.1	41.6 - 42.7	7.4	-0.23 ± 0.30	-1.28 ± 0.50	92 ± 30	63 ± 31
2	35.9	33.1 - 37.6	63.9	0.00	0.00	71 ± 5	56 ± 4
3	26.9	25.2 - 30.3	33.6	-0.01 ± 0.06	-0.14 ± 0.09	31 ± 24	23 ± 6
4	24.1	22.4 - 24.1	23.7	-0.02 ± 0.09	-0.08 ± 0.13	62 ± 21	16 ± 4
5	16.1	13.9 - 17.3	23.0	0.01 ± 0.10	0.05 ± 0.15	—	<10
6	12.2	11.1 - 13.3	20.2	0.14 ± 0.07	0.46 ± 0.10	89 ± 12	32 ± 6
7	0.9	-0.3 - 2.0	15.9	-0.01 ± 0.15	0.13 ± 0.21	78 ± 60	29 ± 25

^aSR velocity of maser component peak (used for polarization analysis).

^bRange of velocities used for position analysis.

^cThe relative positions with respect to the brightest maser component, number 2.

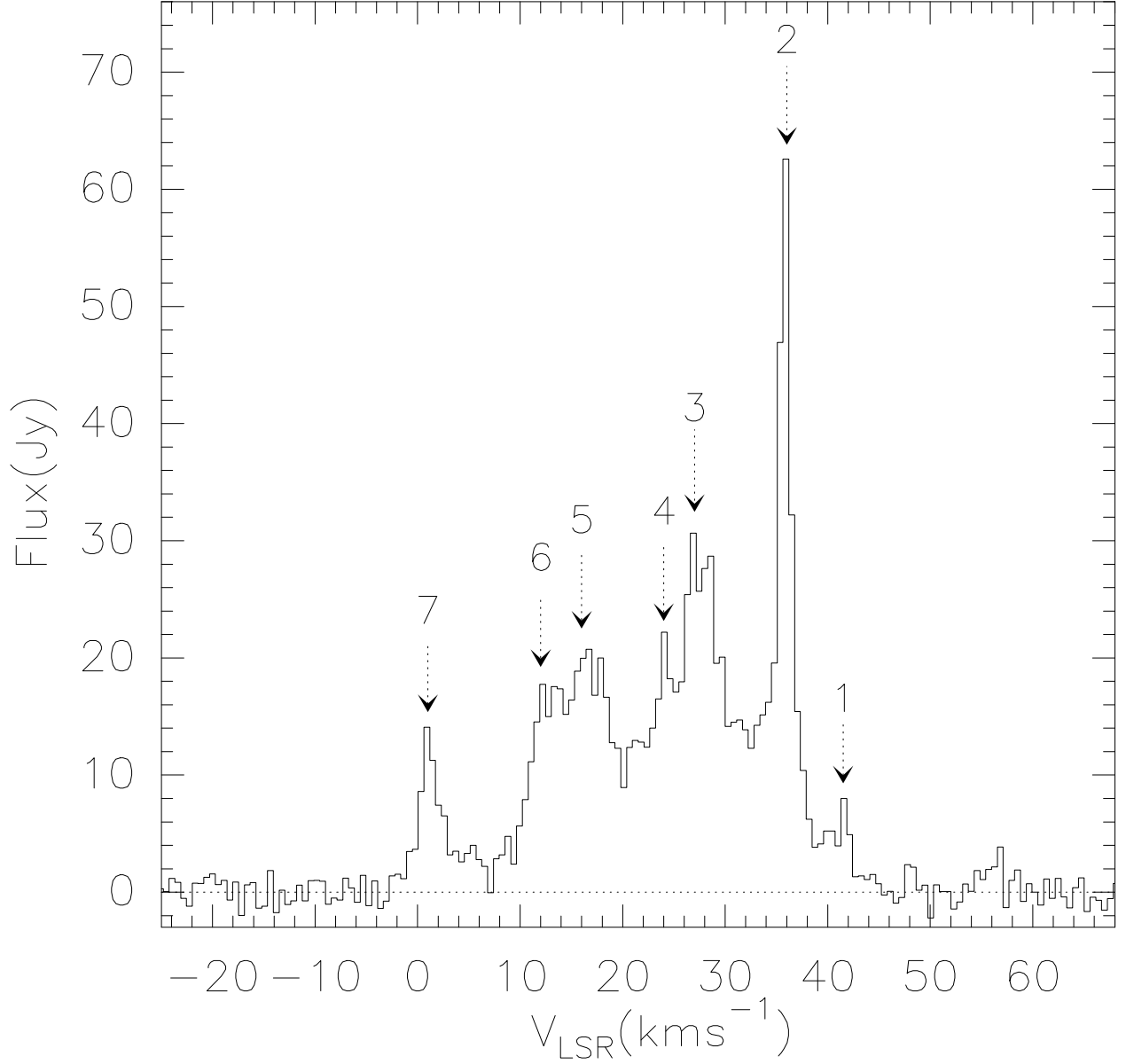


Fig. 1.— An integrated spectrum of the SiO high J maser ($v = 1$, $J = 5 - 4$) associated with VY CMa made from the sum of all observations at various position angles. The velocity axis (radio definition) is measured with respect to the Local Standard of Rest. The stellar velocity is about 20 km s^{-1} . There are probably additional components at 48 and 56 km s^{-1} , which were too weak for detailed analysis. The numbers with arrows identify the seven major components.

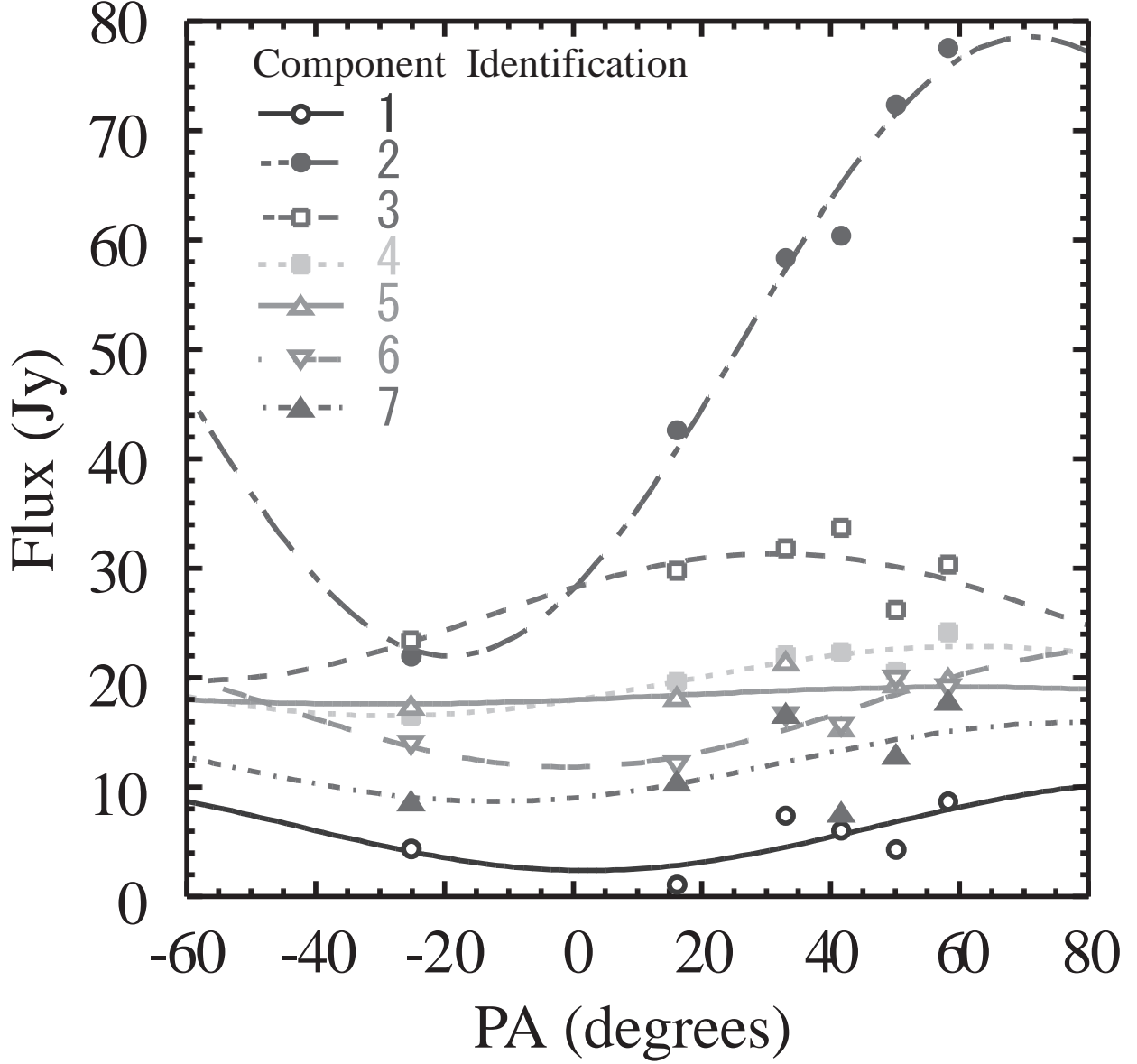


Fig. 2.— The apparent flux density of seven velocity components as a function of the position angle of the feed polarization. The flux density of component 5 was almost constant over the PAs , the flux of the other six components changes as a function of PA because of their linear polarization. No fine gain adjustments were made in the data presented here (see Section 3.1).

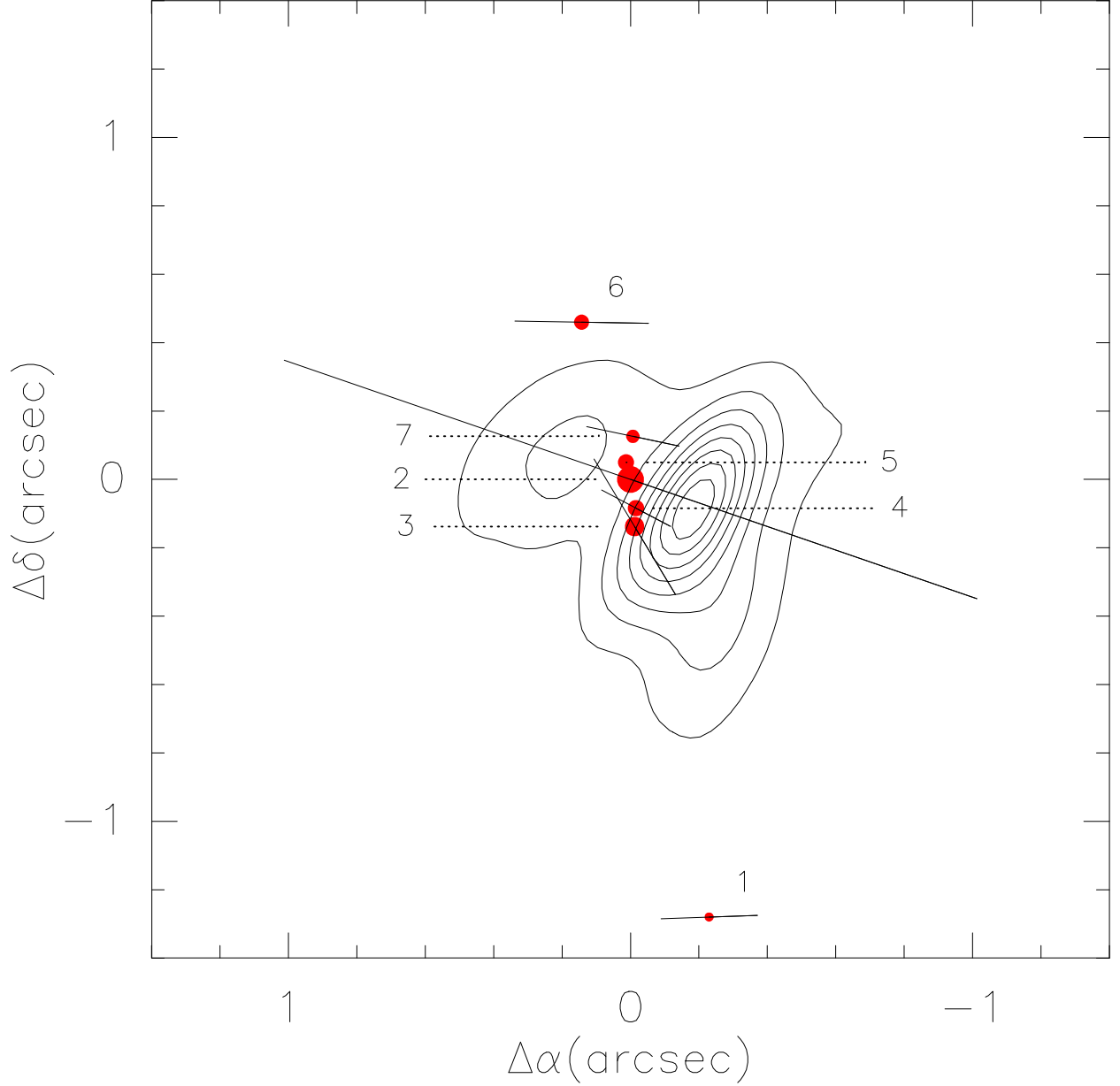


Fig. 3.— Distribution of the SiO ($v = 1$, $J = 5 - 4$) maser components, overlaid on the VLA image of the SiO ($v = 0$, $J = 1 - 0$) emission (Shinnaga et al. 2003). The absolute position of maser 2 is $\text{RA(J2000)} = 7^h 22^m 58.31^s \pm 0.03^s$, $\text{Decl.(J2000)} = -25^\circ 46' 3.''2 \pm 0.''5$. The area of each spot is proportional to its flux density. The line lengths are proportional to the polarized flux density. Only maser 6 (the most northerly component), and possibly maser 1 (the most southerly component) have statistically significant offsets from the position of maser 2 (see Table 1). The mean polarization angle is $72 \pm 4^\circ$. None of the deviations from this mean are significant, except perhaps for masers 3 and 6 (see Table 1).